UPGRADES OF BEAM DIAGNOSTICS IN SUPPORT OF EMITTANCE-EXCHANGE EXPERIMENTS AT THE FERMILAB A0 PHOTOINJECTOR

A.H. Lumpkin, A.S. Johnson, J. Ruan, J. Santucci,Y.-E. Sun, R. Thurman-Keup, and H. Edwards
Fermilab, Batavia, IL U.S.A. 60510

Abstract

The possibility of using electron beam phase space manipulations to support a free-electron laser accelerator design optimization has motivated our research. An ongoing program on demonstrating the exchange of transverse horizontal and longitudinal emittances at the Fermilab A0 photoinjector (A0PI) has benefited recently from the upgrade of several of the key diagnostics stations. Accurate measurements of these properties upstream and downstream of the exchanger beamline are needed. Improvements in the screen resolution term and reduction of the system depth-of-focus impact by using YAG:Ce single crystals normal to the beam direction will be described. The requirement to measure small energy spreads (<10 keV) in the spectrometer and the exchange process which resulted in bunch lengths less than 500 fs led to other diagnostics performance adjustments and upgrades as well.

INTRODUCTION

It is recognized that beam manipulations such as a flat beam transformation followed by an emittance exchange (EEX) could support a high gain free-electron laser (FEL) push to shorter wavelengths [1,2]. An ongoing program on demonstrating the exchange of transverse horizontal and longitudinal emittances at the Fermilab A0 photoinjector (A0PI) has benefited recently from the upgrade of several of the key diagnostics stations. The experiments rely on accurate measurements of these properties upstream and downstream of the exchanger beamline. At gamma ~30 the nominal transverse beam sizes of 1 mm were not an imaging challenge, but the use of an array of 50-micron wide slits to sample the phase spaces to measure divergences of less than 100 microradians resulted in 20 times smaller images with positions distributed over several mm (which approached the resolution and depth-of-focus limits of the initial system, respectively). Improvements in the screen resolution term and reduction of the system depth-of-focus impact by using YAG:Ce single crystals normal to the beam direction will be described.

On the longitudinal side, the requirement to measure small energy spreads (<10 keV) in the spectrometer and the exchange process which resulted in bunch lengths less than 500 fs impacted the corresponding diagnostics performance specifications as well. Upgrades to the Hamamatsu C5680 streak camera and the addition of the Martin-Puplett interferometer addressed the short bunch lengths. An example of the EEX results obtained with the upgraded diagnostics will be presented.

*Work supported by U.S. Department of Energy, Office of Science, Office of High Energy Physics, under Contract No. DE-AC02-06CH11357.

EXPERIMENTAL BACKGROUND

The tests were performed at the Fermilab A0 photoinjector facility which includes an L-band photocathode (PC) rf gun and a 9-cell superconducting radiofrequency (SCRF) accelerating structure which combine to generate up to 16-MeV electron beams [3,4]. The drive laser operates at 81.25 MHz although the micropulse structure is usually counted down to 1 MHz. Due to the low electron-beam energies and OTR signals, we typically summed over 50 micropulses with 0.25 nC per micropulse.

Fundamental to the observations of EEX were the careful beam transport and characterization of the transverse and longitudinal emittances before and after the process. The A0PI beamlines provided these capabilities through a set of rf beam position monitors (BPMs) and optical diagnostics stations as shown in Fig. 1. These imaging station crosses denoted with an "X#" use either optical transition radiation (OTR) and/or scintillator converter screens. Since the initial report of observation of EEX [5], we have upgraded all of the divergence and spectrometer stations to dramatically reduce the magnitude of needed corrections to the simple image sizes that relate to beam size, divergence, or energy spread depending on the diagnostics configuration. All data were obtained with a micropulse charge of 250 pC, but in some cases 10-50 micropulses were used in a single macropulse integrated by the camera CCD chip. The former YAG:Ce 50-μm thick powder screens oriented at 45 degrees to the beam direction [6] (with a revised resolution term of 60± 20μm) have been now replaced by 100-μm thick YAG:Ce single crystals oriented normal to the beam followed by a 45 degree mirror to direct the radiation to the optical system. This configuration should reduce the screen resolution term to less than 10 μm rms based on previous reports [7,8] and also basically eliminate the depth-of-focus issue of the 45 degree scintillator for multiple slit images spread across several mm of the field of view. Energizing a downstream horizontal bending dipole sends the beam into a final beam dump and

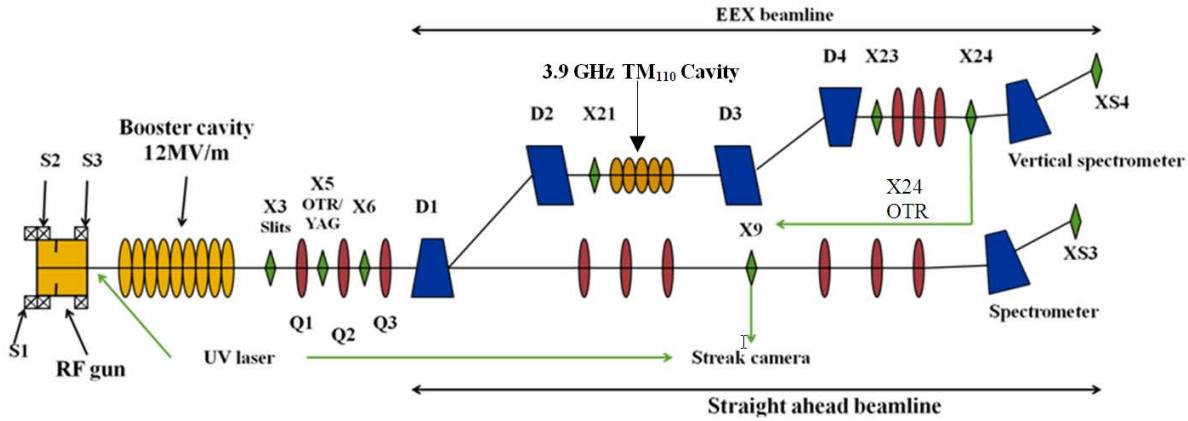

Figure 1: A schematic of the A0 photoinjector test area showing the PC rf gun, 9-cell booster cavity, transverse emittance stations, the OTR stations, the streak camera, and the EEX beamline with the two doglegs.

provides a spectrometer capability when combined with imaging of the beam size at the XS3 dispersive point in the focal plane. (This effect was subsequently also addressed for beam image location in the direction perpendicular to the energy-dispersive direction in the spectrometers by the same configuration change.) The dispersion in x is 324 mm, and the CCD calibration factor is 47.5 μm per pixel. This means a 0.1 % energy spread would correspond to an ~324-μm beam size after corrections are done. The initial sampling station was chosen at X3, and an optical transport system using a 50-mm diameter field lens and a flat mirror brought the light to the firewire digital CCD camera.

In addition, a larger drift length for the initial divergence measurements was attained by using the X05 and X06 stations (drifts of 0.79 and 1.29 m, respectively) instead of X04 and X05 to view the slit images whose sizes were now dominated by the divergence term contribution. The camera edge resolution function terms were evaluated with standard line-pair patterns and were typically about 40-45 μm, and the rms contribution of the finite slit width size was evaluated as 16 μm. These were subtracted in quadrature from the observed slit image profile sizes. So the projected beam sizes were recorded at X3 using OTR, and then vertical and horizontal slit assemblies were inserted in sequence at this position per the slits emittance measuring technique [9]. These were 3-mm thick tungsten plates separated with spacers to form 50-μm wide slits. The depth of metal was chosen to provide strong opacity to the 14.3-MeV beam. A MatLab-based program calculated the emittances and Courant-Snyder (C-S) parameters (α,β,γ) based on the X3-X5 and X3-X6 image pairs [10].

Alternatively, the 4-dipoles of the emittance exchange (EEX) line could be powered and experiments done at an OTR Cross X23 after the fourth dipole and at a drift of 0.56 m to Cross X24. The latter has both OTR and YAG:Ce crystal screen options.

The OTR converter was an Al-coated optics mirror with an 1.0-mm thick glass substrate, and was mounted with its surface normal at 45 degrees to the beam direction on a stepper assembly. The X24 assembly provided vertical positioning with an option for a YAG:Ce crystal scintillator position. The charge was monitored by an upstream current monitor.

SYSTEM RESOLUTION EFFECTS

There are several contributions to the observed beam image size. When they are uncorrelated, the terms can be added in quadrature as described by Lyons [11]. The terms that have been considered are: actual (Act) image size, camera resolution (cam), YAG:Ce powder screen effects (YAG), and the finite slit width (slit) as shown in Eqs. 1, 2. In the spectrometer we must consider the finite size without dispersion, $\beta_x\varepsilon_x/\gamma$ (where γ is the Lorentz factor and ε_x is the normalized x emittance), the dispersive term-energy spread product ($\eta_x\sigma_E$), and the system terms in Eqs. 3,4.

$$Obs^2 = Act^2 + YAG^2 + cam^2 + slit^2 \quad (1)$$

Solving for the actual beam size we have,

$$Act = [Obs^2 - YAG^2 - cam^2 - slit^2]^{1/2} \quad (2)$$

and in the spectrometer,

$$Obs^2 = Act^2 + YAG^2 + cam^2 + \beta_x\varepsilon_x/\gamma \quad (3)$$

Solving for the actual beam size we have,

$$Act = [Obs^2 - YAG^2 - cam^2 - \beta_x\varepsilon_x/\gamma]^{1/2} = \eta_x\sigma_E \quad (4)$$

However, in the case of the divergence measurements based on the slit sampling, we have determined that the depth of focus of the optical arrangement was nonideal. If one samples the phase space with 1-mm spacing, the outer slit images are blurred by the degraded system resolution. This effect is graphically illustrated in Fig. 2, where we see that the observed slit image size variation across the field of view can be reproduced by adding the optical bench based camera resolution term in quadrature with the minimum slit image seen at the focus for the X5 cases. An even larger effect was seen at X24 where the slit spacings were 4 mm. To address such depth-of-focus effects in A0PI stations we have installed at both X5 and X24 in late December 2009 a YAG:Ce single crystal with its surface plane normal to the beam direction and with a 45 degree mirror just downstream which directs the light to the optics. The resulting slit images were more uniform in size across the scene, and averaged divergences and thus calculated emittances were lower in subsequent tests.

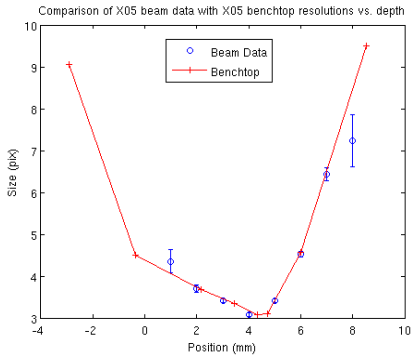

Figure 2: Comparison of the observed vertical slit-image sizes and calculated sizes from the bench tests depth-of-focus data added in quadrature with the minimum beam size at focus for X5.

EXPERIMENTAL RESULTS

Following our implementation of the diagnostic station upgrades, we returned to the basic EEX experiments. Example beam images are shown in Fig. 3a,b for the screens X3 and X5. The beam image and slit image profiles were fit to Gaussian shapes as shown in Figs. 3c,d. Typical full image sizes were 1-2 mm, but the slit images can be as small as 100 μm corresponding to ≈ 80 μrad divergence. The partition of beam size and divergence was adjustable by variation of the solenoidal fields.

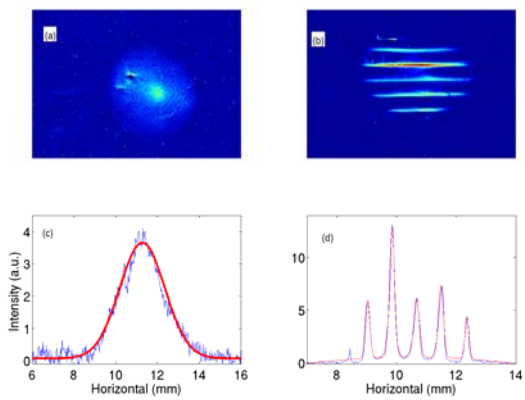

Figure 3: Composite display of a) X3 OTR image, b) X5 YAG:Ce crystal slit images, c) projected x profile (blue) and its Gaussian profile fit (red curve) and d) slit image x profiles with the Gaussian fitted curves (red). The camera was rotated 90 degrees for the images.

Additional X3-X5 results are shown in Fig. 4. The partition of beam size (red circles) and divergence (blue triangles) varied with main solenoid current while the x emittances (black circles) were calculated as 2.0-2.6 mm mrad. The lowest divergence numbers result from large fractional corrections for the camera resolution term. The revised X6 station with a larger drift distance will ameliorate this issue.

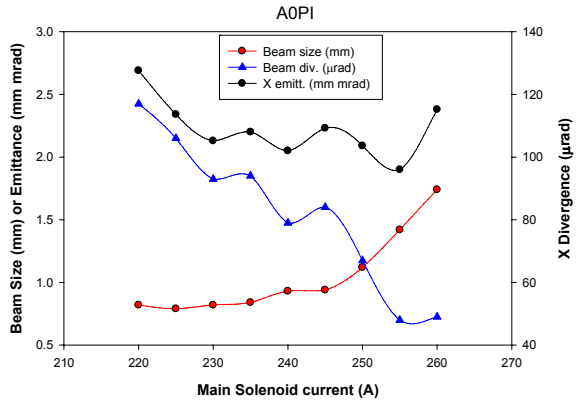

Figure 4. The variation of beam size (red circles), divergence (blue triangles), and normalized emittances (black circles) at X3-X5 versus the main solenoid current (1-06-10).

EMITTANCE EXCHANGE RESULTS

The incoming longitudinal emittance was determined by tuning the 9-cell rf phase for minimum energy spread as observed at the XS3 screen in the straight line spectrometer. At this phase setting, the bunch length was determined at the X09 OTR screen using a Hamamatsu C5680 streak camera operating with synchroscan vertical plugin unit phase locked to 81.25 MHz [12]. The standard input optics barrel using transmissive fused silica lenses was replaced with a reflective mirror optics configuration to reduce the contributions of chromatic temporal dispersion to the observed bunch lengths. Typical energy spread and bunch length 1-sigma values are 8-10 keV and 3 ps or 0.9 mm, respectively. Under the assumption of an upright longitudinal phase space, the product of these rms values would give longitudinal emittance.

For the outgoing transverse emittances, the beam size was first determined at X23, and then with the slit assemblies subsequently inserted at X23 the slit images were measured at X24. The X23-X24 image pairs were used with a drift of 0.58 m. The outgoing emittances and C-S parameters were calculated with the same MatLab program used for the input emittances. The x-emittance was noticeably larger due to the exchange while the y emittance was only 50% larger than initially.

The outgoing longitudinal emittance was evaluated by an energy-spread measurement at the XS4 screen in the spectrometer and by the bunch-length measurement at X24 with the OTR transported to the same streak camera as used at X09 and/or with the FIR CTR transported to a Martin-Puplett interferometer [13]. After the exchange, bunch lengths are typically sub-ps and the energy spread is about 8-10 keV. The interferometer's pyroelectric sensors can also be used to make quick, but uncalibrated relative bunch-length measurements. These were very useful in mapping the effects of the input quadrupole fields on bunch length. Due to optics constraints and the limitations of the longitudinal measurement (i.e., no deflecting cavity), it was difficult to establish without ambiguity the required upright phase-ellipse conditions so

we only have an upper limit formed by the product of the projected components. Examples of the OTR streak image and bunch length profile at X24 with the 5-cell cavity off (left) and on (right) are shown in Fig. 5. The initial bunch length sigma was 2.1 ps and the EEX one was ~0.7 ps. Fig. 6 shows the tracking of 25 shots with the cavity off (red dots) and on (blue squares). The results are quite consistent, but the scatter of points is larger in the cavity-on data since the corrections to the raw data are fractionally larger than for the cavity-off data. The intrinsic camera resolution is 0.6 ps for a red laser source.

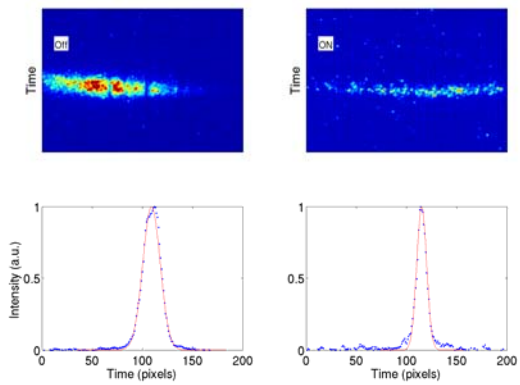

Figure 5: Initial comparison of the OTR streak images taken at X24 with the 5-cell cavity power off (left) and on for EEX (right). The projected temporal profiles are shown below the images, respectively. The red curve is the Gaussian fit to the data profile in each.

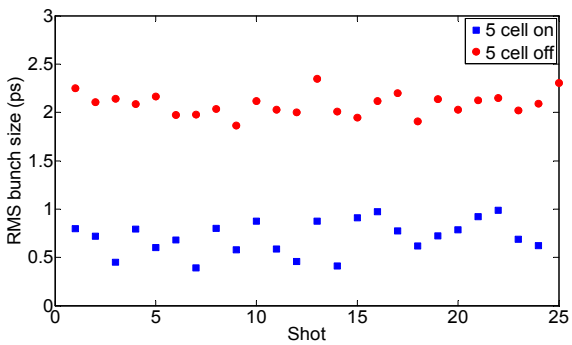

Figure 6: Comparison of the streak camera results at X24 for the 5-cell cavity off (red dots) and on (blue squares) when the exchange was tuned for minimum delta t.

We proceeded to test emittance exchange, and took advantage of the new crystal at X24 as well to measure the outgoing transverse parameters. The initial EEX results (with some image clipping at X23 still to be assessed) from Jan. 5-8, 2010 tests are:

$$\varepsilon^{n}{}_{x} = 2.6 \pm 0.3 \text{ mm mrad} \rightarrow 11 \pm 2 \text{ mm mrad}$$
$$\varepsilon^{n}{}_{z} = 11.5 \pm 1.5 \text{ mm mrad} \rightarrow 5 - 6 \text{ mm mrad}$$
$$\varepsilon^{n}{}_{y} = 2.5 \pm 0.3 \text{ mm mrad} \rightarrow 3.7 \pm 0.3 \text{ mm mrad}$$

The longitudinal-to-transverse(x) exchange and the transverse(x)-to-longitudinal exchange are clear, albeit with some growth in the latter which is partially explained in a transport matrix model including space charge effects [14]. The vertical emittance growth is about 50% perhaps due to some coupling between the x-y planes. The statistical errors are calculated in the emittance code [10].

SUMMARY

In summary, we have investigated the contributions of several terms to beam profile station system resolution at A0PI and converted most of the YAG:Ce powder screens to YAG:Ce single crystal screens. We have also changed the geometry of the screens at the divergence stations to eliminate the compromising depth-of-focus issues across the field of view. These diagnostic upgrades have resulted in more reliable characterization of the transverse and longitudinal emittances before and after EEX.

ACKNOWLEDGEMENTS

The authors acknowledge the beamline vacuum work of W. Muranyi and B. Tennis and support from M. Wendt and M. Church of Fermilab.

REFERENCES

[1] M. Cornacchia and P. Emma, "Transverse to Longitudinal Emittance Exchange", Phys. Rev. ST-AB **5**, 084001 (2002).
[2] P.Emma, Z. Huang, and K.-J. Kim, Phys. Rev. ST-AB **9**, 100702 (2006).
[3] J.P. Carneiro et al., Proc. of PAC99, 2027 (1999).
[4] Timothy W. Koeth, "An Observation of a Transverse to Longitudinal Emittance Exchange at the Fermilab A0 Photoinjector", Ph. D. dissertation, May 2009.
[5] Timothy W. Koeth et al., "Emittance Exchange at the Fermilab A0 Photoinjector",Proc. of PAC09, JACoW.
[6] A.H. Lumpkin et al., "Spatial Resolution Limits of YAG:Ce Powder Beam profile Monitors at the Fermilab A0 Photoinjector", Proc. of FEL09 Liverpool UK, JACoW (2010).
[7] B.X. Yang (private communication of x-ray results).
[8] M. Maesaka et al., "Beam Diagnostic System of XFEL/Spring8", Proc. of DIPAC09, JACoW (2009).
[9] C.H. Wang et al., "Slits Measurement of Emittance on TTF", International Conference on Accelerator and Large Experimental Physics Control Systems, Trieste, Italy (1999).
[10]R. Thurman-Keup, Emittance code for A0PI, 2009.
[11]L. Lyons, *Statistics for Nuclear and Particle Physicists* (1986).
[12]A.H. Lumpkin and J. Ruan, "Initial Synchroscan Streak Camera Imaging at the A0 Photoinjector", Proc. of BIW08, Lake Tahoe,CA, JACoW (2009).
[13]R. M. Thurman-Keup et al., "Bunch Length Measurements at the Fermilab A0 Photoinjector", Proc. of the BIW08, Lake Tahoe CA (2008).
[14]A.S. Johnson et al., "Demonstration of Transverse-to-Longitudinal Emittance Exchange at the Fermilab Photoinjector", submitted to IPAC10, Kyoto Japan.